Compression and Recovery Behaviour of Polyamide-6 Based Foams

V.G. Izzard[*], H. Hadavinia[*1], V.J. Morris[*], P.J.S. Foot[*], L. Wilson[**] and K. Hewson[**]
[*]Materials Research Centre, Kingston University, London, UK
[**]Zotefoams plc, Croydon, UK

Received: 30 August 2011, Accepted: 21 December 2011

SUMMARY

This paper presents experimentally determined compression sets and compression behaviour of two closed-cell, crosslinked foam materials; ZOTEK N B50 (Nylon 6) and ZOTEK N A30 (nylon/polyolefin alloy). This work forms the basis of future investigations into the post-impact behaviour of these foams.
Compression set performance was measured at 25.0, 37.5 and 50.0% strain at nine temperatures ranging from -5 to 90 °C. Compression tests at constant strain rates were conducted at four temperatures between 23 to 90 °C. Finally compression tests at 23 °C were repeated at four strain rates between 0.3 and 550 hr^{-1} to determine strain rate dependency. The Nagy and Williams-Landel-Ferry scaling factor for strain rate and temperature were applied to the experimental results and equations were derived which allowed the performance of the two polyamide based foams to be interpolated over the strain rate and temperature range of study. The required material properties of interest of the base polymers have been assessed and are presented and discussed in relation to the performance of the foam materials.

Keywords: Cellular solid, Polyamide, Nylon-6, Polyolefin, Compression set, Stress-strain, Scanning electron microscope, Glass transition temperature, Strain rate, Foam

1. INTRODUCTION

Polymer foams are multi-phase materials made of a matrix material (polymer) and cells (gas). Depending on the matrix material as well as the cell microstructure, foams exhibit dramatically different properties. In the majority of polymer foam applications such as automotive, sport and packaging, foams are subjected to stresses. Recovery after relaxation of an applied stress is an important property in the subsequent behaviour of the foams. In addition, one of the primary uses for polymer based cellular solids is to act as energy-absorbing materials during impact. In reality, impacts occur over a wide range of temperatures and at velocities that may vary over many orders of magnitude and at angles of incidence that are unpredictable. Understanding the behaviour of the foam requires detailed characterisation of the foam material's response. Many authors, including Mills[1], Gibson and Ashby[2], have reported on work that characterises cellular solids at the micro level using structural mechanics modelling based on assumed lattice structures. As stated by Kraynik and Warren[3], the mechanical behaviour of cellular solids is dependent on the mechanical behaviour of its components. That is to say, in order to predict foam performance, the models developed must be based on an accurate description of the base polymer behaviour. However, many of these models assume that variations in base polymer properties are either simply characterised or linearly dependent with regard to environmental conditions[4,5], and therefore cannot be applied to a range of foams[5] or situations.

As given by Mills *et al.*[6] and Rodriguez-Perez *et al.*[7], it is well established that the driving forces for recovery of closed cell foams are related to (i) the compressed gas inside the cells and (ii) the viscoelastic recovery of the deformed cell walls. Additionally, it is also widely known that the mechanical properties of the base polymers are sensitive to both temperature and strain rate, especially at or near to their glass transition temperatures (Tg)[8]. It is therefore crucial that any cellular solid performance predictions are based, not only on the understanding of the micro structure, but also on a detailed knowledge of the base polymer behaviour. For any model to be truly useful it must consistently and realistically predict the foam performance over a wide range of conditions. Of equal importance is the foam behaviour during post-compression recovery. A robust model should be consistent over a range of temperatures with regard to these parameters. This study

[1]Corresponding Author: e-mail: h.hadavinia@kingston.ac.uk (H. Hadavinia),
Tel.:+44 20 8417 4864, Fax:+44 20 8417 4992

provides a range of experimental measurements fitted by scaling and empirical equations to allow predictive interpolation of static compressive behaviour as a precursor for future studies into the dynamic performance of these materials.

Zotefoams plc is a world leader in the manufacture and distribution of speciality foam materials, manufactured using a unique, proprietary technology[9]. The technology uses nitrogen gas as a Physical Blowing Agent (PBA) which is dissolved into the base polymer in a high pressure/temperature process. Once equilibrium is achieved, thermodynamic instability is introduced to initiate nucleation of the foam structure. This method of production minimises impurities in the product whilst also optimising properties and performance. It is also considered environmentally friendly since nitrogen is the only major by-product of the process. A further advantage of this technology is the wide range of materials to which it can be applied.

Examples of such materials are the newly developed closed cell foams based on Polyamide-6 (PA6) under study here. For materials such as PA6, foaming has traditionally been technically challenging with limitations on any possible reduction in density. ZOTEK N B50 and ZOTEK N A30 grade foams have nominal densities of 50 kg/m^3 and 30 kg/m^3, respectively. The characteristics of these foams reflect the general properties of this class of polymer with good high temperature performance, resistance to hydrocarbon fuels and oils combined with impact performance, buoyancy and low thermal conductivity which derive from the cellular structure. These foams are considered ideal for shock and impact absorption, acoustic dampers and cushioning applications in extreme environmental conditions.

2. BASE POLYMER PROPERTIES

The fundamental behaviour of any cellular solid is influenced by the properties of the base polymer. To predict the mechanical performance and possible responses of the foam, it is important to gain an understanding of the polymer properties matrix. These properties are essential for further numerical studies for modelling of the foams under general multiaxial loading.

2.1 Experimental Procedure

Tensile tests were undertaken on base polymer samples of both foam materials to determine the ultimate tensile stress, elongation at break, elastic modulus in tension and Poisson's ratio.

For each base polymer, three tensile tests were carried out with reference to BS 2782-3 standard[10]. Strain measurements were made using two VISHAY general purpose strain gauges CEA-06-240UZ-120. A third strain gauge was used to determine Poisson's ratio of the material, **Figure 1a**. These gauges have a stated accuracy of 0.1% which far exceeds the accuracy of 2% in measurements, as required by BS 2782-3. Load and strain data were recorded using VISHAY data logging system 5000 operating at 10Hz.

All dimensional measurements were carried out using a MID-F125/150 Mitutoyo Digimatic digital micrometer with an accuracy of ±0.006 mm fitted with an 8 mm flat anvil. For mass determination, a Mettler AJ150 balance with an accuracy of ±0.001 g was used. Prior to testing, all samples were conditioned at 23 °C and 50% RH for a minimum of 24 hours, but no control of humidity was applied during the testing.

The glass transition temperature (Tg) was measured on the base polymers using differential scanning calorimetry (DSC). A small amount of material (circa 5 mg) was sealed in an aluminium DSC crucible using a pierced lid. The samples were heated in turn from -100 to 180 °C, and then cooled back to -100 °C before reheating the sample back to 180 °C. Heating and cooling rates of 10 °C/min were used throughout.

2.2 Results of Base Polymer Investigation

The mechanical properties of both base polymers are shown in **Table 1**. These are based on the mean of three separate measurements for each material. The tensile stress-strain curves of N A30 and N B50 are shown in **Figure 1b**. The elongation to break and elastic modulus for the N A30 base polymer show it is significantly more ductile than N B50 but has lower stiffness. It would be expected that the foam materials would also demonstrate similar differences at equivalent density. The properties presented in **Table 1** are consistent with previously published data[11,12].

3. FOAM PERFORMANCE

3.1 Compression Set

Compression set is a standard test procedure applied to foams. It provides data on one of the basic mechanical responses of foams: recovery after fixed compressive strain loading. In literature, there are many instances where compression set tests have been used to monitor the effects on foams following chemical or mechanical ageing or when process/formulation variations were being investigated. For example, the effects of blending two or more polymers[13,14], the effect of the addition of fillers[15,16], the effect of the level of crosslinking[17] and aspects of foam ageing[18,19]. Little however has been reported on the data from the compression set test itself, or on compression set data outside the scope defined by the most commonly used ISO[20] and ASTM[21] standards. Often compression set data are recorded at only a few points of recovery time,

and no predictive interpretation of the foam performance outside of the range of these measurements is available.

Literature does contain studies on recovery rates after loading for crosslinked, closed-cell foams. Mills and Gilchrist[22] investigated the recovery rates of low density polyethylene (LDPE) and ethylene vinyl acetate copolymer (EVA) foams on completion of 7 day creep tests. Their work shows that at relatively high strains, the majority of the gas in the cells escapes. For low density foams, viscoelastic recovery is hindered by the pressure drop in the cells, making recovery a slow process. This study does not investigate the permeability of cell walls to air but it is a likely contributing factor to the recovery of the foams studied in this work.

3.1.1 Compression Set Experimental Procedure

In order to reduce equipment-dependent uncertainties, all dimensional measurements were carried out in accordance with ISO 1923[23] using a MID-F125/150 Mitutoyo Digimatic digital micrometer with an accuracy of ±0.006 mm fitted with an 8 mm flat anvil. For mass determination, a Mettler AJ150 balance with an accuracy of ±0.001 g was used. The density of the foam sheet was calculated according to ISO 845[24]. To minimise the effects of density variation upon the results, all samples were taken from two foam sheets manufactured in the same batch. These samples were conditioned for a minimum of 6 days at 23 °C (±2 °C) and 50% (±5%) relative humidity prior to testing.

Compression set tests were conducted in accordance with ISO 1856[20]. Three samples were tested for each test condition and the mean value reported. Nominal test sample size was 50 mm × 50 mm × 25 mm. The dimensions of the ZOTEK N B50 and ZOTEK N A30 samples were recorded and compressed

Figure 1. (a) Tensile test specimen of base materials, (b) Stress-strain behaviour of N B50 and N A30 base polymer

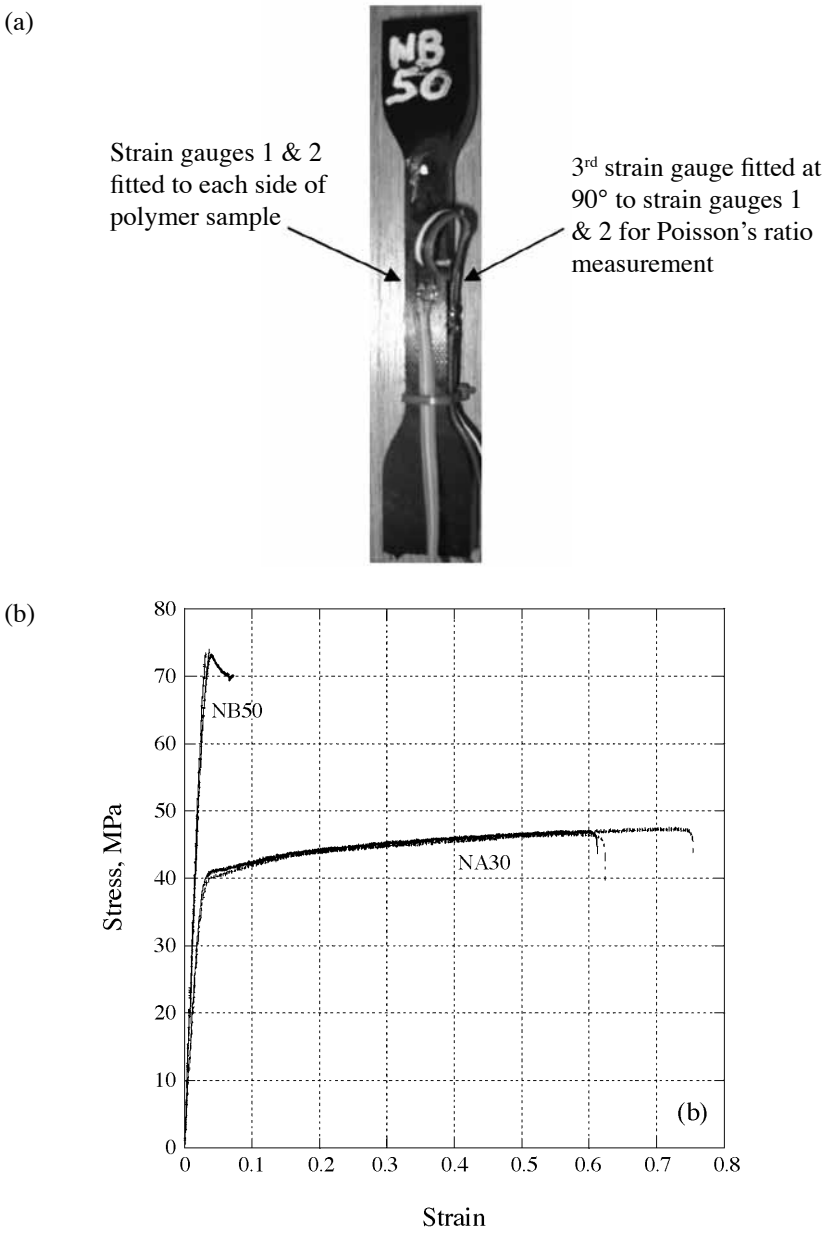

Table 1. Base polymer properties at 23°C

Property*	Nylon-6 N B50		Nylon /Polyolefin Alloy N A30	
		Standard Deviation		Standard Deviation
Density (kg/m^3)	1143	3.8	1099	0.4
Elastic Modulus E_s (GPa)	3.19	0.02	2.11	0.01
Max Stress s_s (MPa)	73.9	0.9	47.2	0.4
Poisson's Ratio	0.398	0.001	0.319	0.012
Elongation %	3.4	N/A	66	N/A
Glass Transition Temperature (°C)	45-51			
**Based on the mean of 3 samples*				

to a fixed strain (25.0, 37.5 and 50.0% of original thickness) and acclimatised at experimental temperature (-5, 10, 23, 30, 40, 50, 60, 70 and 90 °C) for a duration of 22 hours.

On release of the strain, the samples were maintained at the relevant experimental temperature during recovery. The dimensions of the samples were re-measured at various time intervals from 30 minutes through to 24 hours post release. Recovery at temperature is beyond the scope of ISO 1856[20].

All compression set (*c.s.*) data are reported according to ISO 1856[20], using Eq. (1)

$$c.s. = \frac{d_o - d_r}{d_o} x100 \quad (1)$$

where d_o is the original thickness of the sample and d_r is the thickness after recovery at times of interest.

3.2 Results of Compression Set Testing

Table 2 provides a comparison of the compression set results for both N B50 and N A30 at the temperature and recovery times specified in ISO 1856[20].

The N B50 results from **Table 2** show good agreement with published data[9]. This confirms that the methods adopted are transferable to additional test conditions and to other polyamide-6 based foams.

Table 2 also shows that the N B50 foam recovers at approximately the same rate for the first 30 minutes of the recovery. This rate is not affected significantly by the level of initial fixed strain.

Figure 2 shows the experimental compression sets as a function of recovery time at various temperatures after initial fixed 50% compression strain for N B50 and N A30. The curves represent the best fit for each

Figure 2. Compression set results of N B50 and N A30 at temperatures between -5 °C and 90 °C at c.s. 50.0%

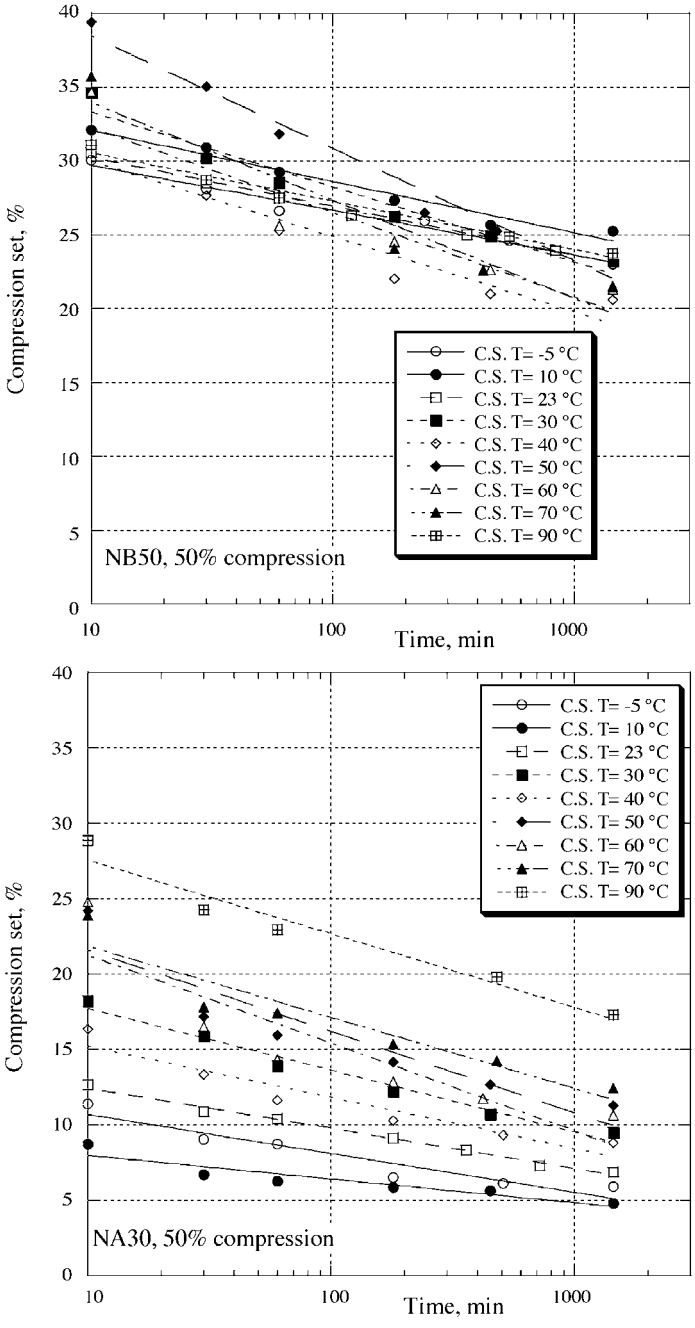

Table 2. Comparison of compression set tests results

Parameter	N B50	N A30
Density	47.96 kg/m^3	31.62 kg/m^3
c.s. (25.0%, 30 min, 23 °C)	14.7%	7.0%
c.s. (25.0%, 1440 min, 23 °C)	10.9%	3.4%
c.s. (37.5%, 30 min, 23 °C)*	22.7%	10.9%
c.s. (37.5%, 1440 min, 23 °C)*	19.3%	7.6%
c.s. (50.0%, 30 min, 23 °C)	28.6%	10.9%
c.s. (50.0%, 1440 min, 23 °C)	23.4%	6.9%
* *Initial fixed strain characteristic not explicitly included in ISO 1856*		

temperature studied. The results show that N B50 has a lower recovery rate than the N A30 across all measured temperatures. A wider spread of data is also noticeable with respect to temperature for N A30. This would suggest that the N A30 recovery is more sensitive to temperature than that of N B50. In addition, the results indicate that neither material returns to a zero compression set state (i.e. full recovery) after 24 h. This is expected, given the short timescale and the closed cell nature of these materials.

As previously reported by Izzard *et al.*[25]; Eq. (2) below is an empirical, predictive equation for recovery after compression set as a function of time for N B50. The present study has extended the temperature range and it also includes 37.5% initial strain.

$$\text{c.s. } (\%) = a \ln(t) + b \quad (30 < t < 1440) \qquad (2)$$

where t is the recovery time in minutes and 'a' and 'b' are temperature dependent coefficients as presented in **Table 3**.

The same conditions are applied to the lower density, N A30 foam material, and results showed a similar pattern to those as previously reported[25]. Eq. (2) can therefore apply to N A30 foam with the temperature-dependent coefficients given in **Table 4**. In both cases the data, when plotted, exhibits a high logarithmic dependency as a function of recovery time.

Eq. (3) predicts the compression set as a function of recovery time at a specific temperature. Although **Figure 2** would indicate a very limited temperature effect on the compression set behaviour for N B50, it shows a definite upward trend for N A30, indicating that a temperature dependent function is required. A surface modelling package, 3D table curve[26], was used to derive a surface fit. Equation (3) uses a 3rd order polynomial for temperature which includes a logarithmic time component.

Figure 3. Comparison of experimental compression set data at 30 and 1440 minutes with empirical curve fit- N A30

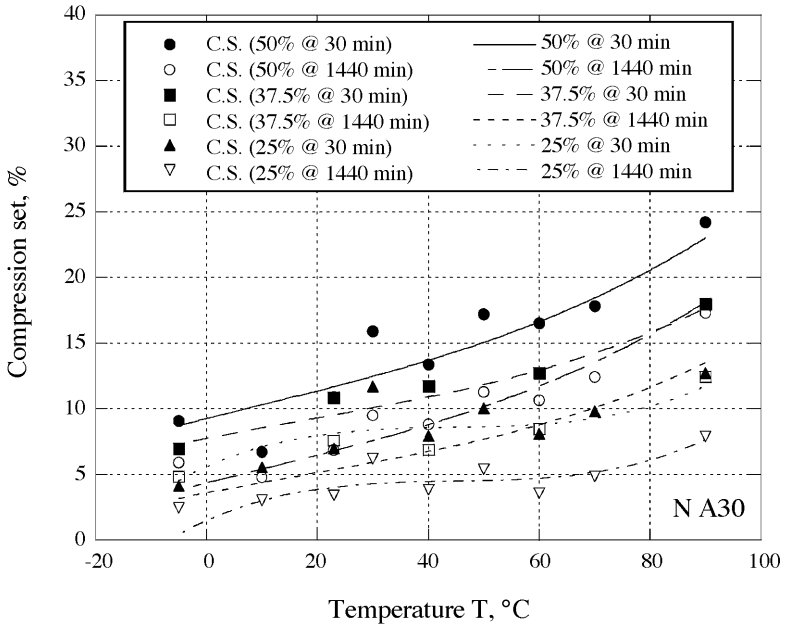

Table 3. Coefficients of logarithmic empirical fitting to compression set data for ZOTEK N B50

Test Temperature (°C)	Compressive Strain = 25.0%		Compressive Strain = 37.5%		Compressive Strain = 50.0%	
	a	b	a	b	a	b
-5	-0.934	16.511	-0.812	21.246	-1.208	32.092
10	-1.340	18.744	-0.619	19.596	-1.497	35.509
23	-1.004	18.339	-0.870	25.699	-1.323	32.884
30	-0.936	20.644	-1.242	25.410	-1.798	36.023
40	-1.224	19.359	-1.827	31.347	-1.855	32.000
50	-1.275	22.352	-1.662	31.238	-3.314	44.367
60	-1.266	22.138	-1.431	29.447	-1.745	33.623
70	-1.050	19.644	-1.200	27.012	-2.334	37.426
90	-1.360	21.431	-1.591	29.680	-1.265	32.904

Table 4. Coefficients of logarithmic empirical fitting to compression set data for ZOTEK N A30

Test Temperature (°C)	Compressive Strain = 25.0%		Compressive Strain = 37.5%		Compressive Strain = 50.0%	
	a	b	a	b	a	b
-5	-0.373	4.997	-0.578	8.857	-0.900	11.986
10	-0.632	7.583	-0.660	8.439	-0.460	8.268
23	-0.961	10.221	-0.827	13.612	-1.093	14.743
30	-1.448	16.435	-1.063	13.043	-1.629	20.955
40	-1.101	11.524	-1.279	15.559	-1.137	16.649
50	-1.215	14.100	-1.417	18.000	-1.548	22.333
60	-1.082	11.427	-1.098	16.148	-1.447	20.754
70	-1.282	14.067	-1.392	19.370	-1.434	22.969
90	-1.326	16.911	-1.598	24.060	-1.731	30.159

This function is an empirical surface fit which predicts the compression set performance of these foams as a function of both temperature and time.

$$c.s.\ (\%) = a + b\,T + c\,T2 + d\,T3 + e\,\ln(t) \quad (-5 < T < 90,\ 30 < t < 1440) \qquad (3)$$

where t is the recovery time in minutes, T is the recovery temperature in °C and 'a' to 'e' are the foam dependent constant coefficients presented in **Tables 5** and **6** for N B50 and N A30, respectively.

Compression set at any given time for N B50 is almost independent of temperature but for N A30 the compression set increases as the temperature rise as shown in **Figure 3**.

3.3 Compression Testing

The compressive stress-strain performance of the foam is a characteristic of its energy-absorbing capabilities, and can be determined by the methods described in BS3386-1[27]. It should be noted that the level of accuracy for force and displacement used in this study far exceeds those specified in the standard. Further to this, BS3386-1 does not include investigation at varying strain rates or environmental temperature. This study used BS3386-1 as a guide and develops the method to study the effect of these parameters.

3.3.1 Experimental Procedure - Effect of Temperature at Constant Strain Rate

All samples were 50 mm diameter 25 mm thick foam cylinders which were conditioned and measured as per Section 3.1.1. Cylinder diameter was measured using Engineer's stainless steel Vernier Calliper to an accuracy of ±0.02 mm.

A sample was placed on an aluminium disc of a slightly larger diameter held by an aluminium rod in the lower jaw of the universal testing machine. A brass tube of length 300 mm was positioned over the sample and located on a preinstalled base cap. A second 50 mm aluminium disc and rod arrangement was placed in the tube and held above the foam sample by the upper jaw of the universal testing machine. The brass tube was capped using a second brass plate. A heating jacket was wrapped around the assembly and set to the required temperature (see **Figure 4**). The brass tube served as a heat sink and dampened the temperature fluctuations of the heating jacket. Temperature was monitored and controlled by the use of thermocouples; one on the foam sample and one in the brass tube. Once thermal equilibrium had been achieved, the sample was left to condition for a further 2 hours.

Compressive loading was applied to the sample at a constant strain rate of 0.01 s^{-1} until a strain of 80%

Table 5. Coefficients of surface fitting to compression set data at various temperatures N B50

Compressive Strain	Coefficient				
	a	b	c	d	e
25.0%	17.7925	8.2464×10^{-2}	-1.0413×10^{-4}	-5.7929 x 10-6	-1.1572
37.5%	23.5808	1.1710×10^{-1}	-1.5032×10^{-5}	-8.9340×10^{-6}	-1.2686
50.0%	35.7303	4.2558×10^{-2}	-2.0852×10^{-3}	-1.7781×10^{-5}	-1.7773

Table 6. Coefficients of surface fitting to compression set data at various temperatures N A30

Compressive Strain	Coefficient				
	a	b	c	d	e
25.0%	9.1989	1.8785×10^{-1}	-4.0553 x10-3	3.0341×10^{-5}	-1.0598
37.5%	11.4089	8.2848 x 10-2	-4.2795×10^{-4}	8.1484×10^{-6}	-1.0745
50.0%	13.5568	1.0628×10^{-1}	-2.0541×10^{-4}	8.0655×10^{-6}	-1.2642

Figure 4. High temperature compression test set up

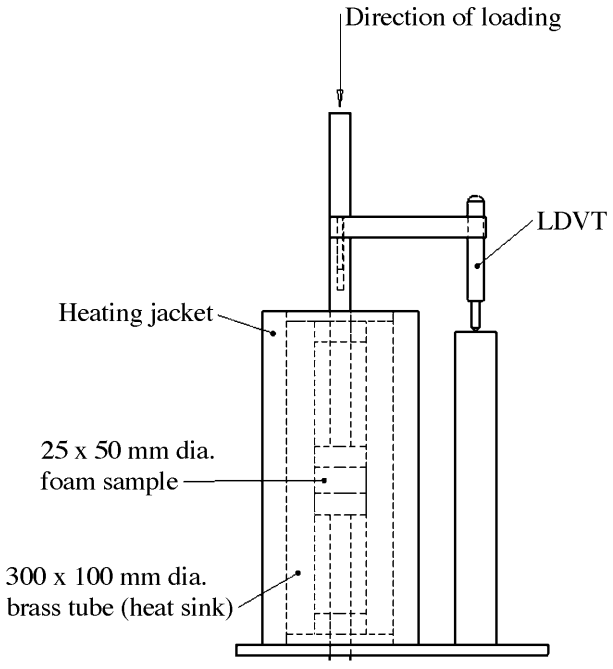

was reached. Compression in the sample was measured using a LVDT branched from the loading arm (see **Figure 4**). Both load and compressive displacement were logged using a Vishay Measurements Group System 5100 (data logger) set at 10Hz sample rate. The foams were tested at four different temperatures of 23, 50, 70 and 90 °C.

3.3.2 Results of Compression Tests - Effect of Temperature at Constant Strain Rate

The compression tests results at different temperatures are shown in **Figure 5**. The elastic modulus of the foam shows a temperature dependency; the higher the temperature, the lower the elastic modulus. The elastic modulus will vary both above and below Tg. Proportional change is lower below Tg than it is above.

The observed temperature dependent compressive stress-strain behaviour of the foams can be described using the Williams-Landel-Ferry (WLF)[28] shift factor:

$$L(T) = EXP\left[\frac{-C_1\left(T - T_r\right)}{C_2 + \left(T - T_r\right)}\right] \quad (4)$$

where C_1 and C_2 are material dependent constants, T_r is the reference temperature (often taken as the polymer glass transition temperature T_g) and T is the temperature of interest.

The compressive behaviour of N A30 does not exhibit the behaviour as predicted by using the shift factor in Eq. (4). It is thought that the change in cell gas pressure due to temperature is the dominating effect, rather than any characteristic of the polymer behaviour. At increasing strain increments, the volume of the cells decreases. Raising the temperature at those strain increments also results in the cell gas pressure being higher. This effect counteracts the temperature 'softening' of the polymer that would normally be

Figure 5. Experimental and fitted stress-strain curves over the temperature range 50 °C to 90 °C. (a) N B50 (b) N A 30

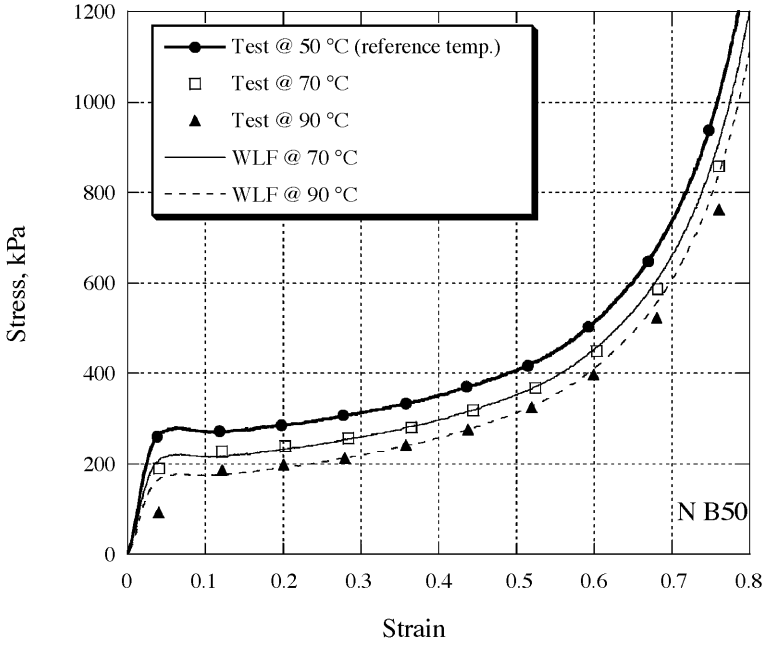

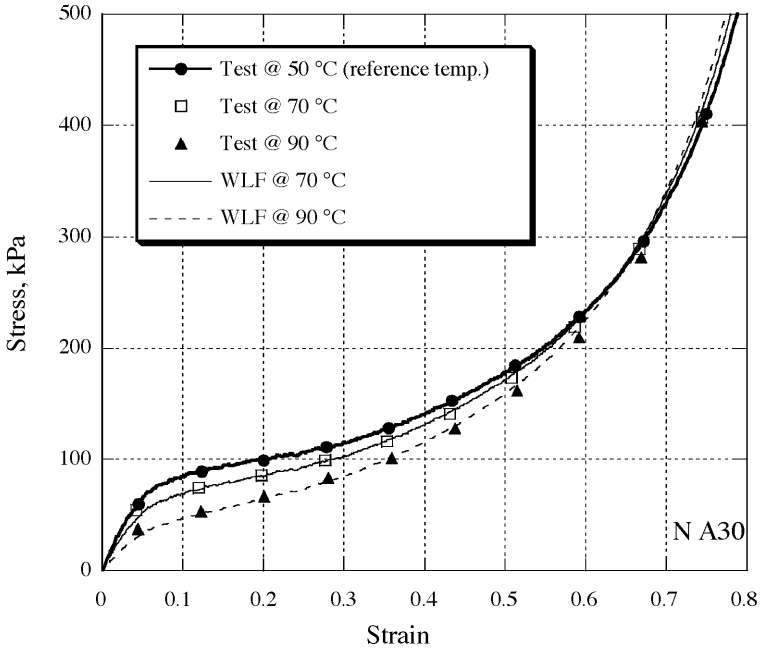

expected. For higher density foams, where there is more polymer in the cell walls or struts, and foams made with stiffer polymers, the gas pressure has a less dominating effect on their buckling capability. Therefore the convergence at higher strains seen in **Figure 5b** is not observed in higher density/stiffer foams. In order to understand the polymer performance in low density and more ductile foams, the gas pressure effect must be extracted from the data prior to the application of the WLF shifting factor.

From the ideal gas law, assuming the number of moles is constant and Poisson's ratio is zero, the gas pressure curves for given temperatures can be determined from Eq. (5):

Cell Gas Pressure (MPa gauge)=

$$\left[\left[\frac{T}{T_o}\right] x \left[\frac{\varepsilon}{1-\varepsilon-\left(\rho_{Foam}/\rho_{Polymer}\right)}\right] x 0.1013\right] \quad (5)$$

where T is the temperature of interest, T_o is the temperature at which the foam cell pressure is in equilibrium with atmospheric pressure, ε is strain, ρ_{Foam} and $\rho_{Polymer}$ are the foam and base polymer densities, respectively.

In this case, T_o is taken to be 23 °C as the foam is conditioned at this temperature. This is to achieve gas equilibrium within the foam.

If the effect of gas pressure within the cell is added to the WLF shifting factor, the stress strain performance of N A30 can be accurately predicted as shown in **Figure 5** using the following equation:

$$\sigma_T(\varepsilon) = \sigma_0(\varepsilon)L(T) + \text{Cell Gas Pressure} \quad (6)$$

where $s_T(\varepsilon)$ is the stress at temperatures of interest between 50 and 90 °C, $\sigma_o(\varepsilon)$ is the stress at the lowest temperature studied above Tg, in this case 50 °C.

Eq. (6) was fitted to N B50 and N A30 experimental data. The relative density is based on foam densities as given in **Table 2**. Constants C_1 and C_2 given in **Table 7** obtained using iterative methods.

3.3.3 Experimental Procedure - Effect of Strain Rate at Constant Temperature

All samples were measured and conditioned as per Section 3.1.1. Foam breadth and width were measured using an engineer's stainless steel Vernier Calliper to an accuracy of ±0.02 mm.

Table 7. WLF coefficients for temperature shifting factor in Eq. (4)

Foam Material	C_1	C_2
N B50	11.0	880
N A30	3.4	180

A single sample, whose nominal dimensions were 25 mm x 140 mm x 140 mm, was tested at each test condition. The load and linear variable differential transducers (LVDTs) outputs were digitally logged using VISHAY data logging system 5000.

The foam sample remained unloaded during this process through the use of 26 mm spacers (see **Figure 6**). The rig was installed into a Mayes, 2 column universal testing machine with a 50 kN load cell. Four LVDTs were fitted to each corner of the test rig and zeroed. The spacers were removed and the sample compressed to approximately 80% of its original thickness. An average displacement from the LVDTs was calculated and used to determine strain. Samples were tested at strain rates between 0.300 to 550 h^{-1} at 23 °C for both N B50 and N A30.

3.3.4 Results of Compression Tests - Effect of Strain Rate at Constant Temperature

The foam elastic moduli E^* at 23 °C for N B50 and N A30 at different strain rates are given in **Table 8** and shown graphically in **Figure 7**. The lines indicate that there was a near linear variation of elastic moduli with log of strain rate over the ranges studied.

Nagy *et al.*[29] stated that based on quasi-static test data, it is possible to model stress as a function of strain and strain rate using the following constitutive equation:

$$\sigma(\varepsilon) = \sigma_0 \left(\frac{\dot{\varepsilon}}{\dot{\varepsilon}_o}\right)^{n(\varepsilon)} \quad (7)$$

where:

σ_0 = Nominal stress at quasi-static strain rate $\dot{\varepsilon}_0$

$\dot{\varepsilon}$ = Strain rate

$\dot{\varepsilon}_0$ = Strain rate at quasi-static test

$n(\varepsilon)$ = Rate dependency coefficient where $n(\varepsilon) = a + b\varepsilon$.

The material rate dependency coefficient $n(\varepsilon)$ was derived by plotting the stress ratio against strain rate ratio on a log-log scale at specific strain levels. As shown in **Figure 8a** for N A30, a family of straight lines with tangent n was formed for both foams. A regression was then used to fit the tangents of these lines, n, against strain. From this the functional form of n is derived as shown in **Figure 8b** for N A30. The results of $n(\varepsilon)$ for N A30 and N B50 are:

$$n(\varepsilon) = \begin{cases} 0.0052 - 0.07424 \log(\varepsilon) & \text{N A30} \\ 0.0785 - 0.0674\varepsilon & \text{N B50} \end{cases} \quad (8)$$

Although the test results scaled accurately for N B50, they did not scale so well for N A30. It was found that N A30 foam softened with increasing strain. This behaviour was not observed for N B50 and therefore no softening at higher strains occurred.

Figure 6. Compression test set up at different strain rates

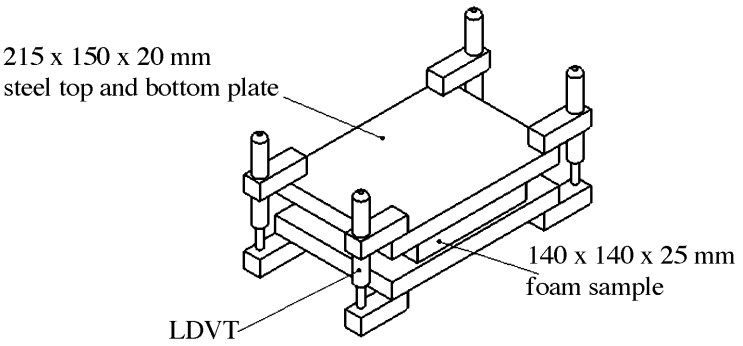

In order to improve the scaling for low stiffness foams, the Nagy equation was modified to include an additional strain-dependent term as follows:

$$\sigma(\varepsilon) = A(\varepsilon)\sigma_0 \left(\frac{\dot{\varepsilon}}{\dot{\varepsilon}_o}\right)^{n(\varepsilon)} \quad (9)$$

where $A(\varepsilon)$ is a linear strain dependent function for low stiffness materials. By using iterative methods it was found that:

$$A(\varepsilon) = \begin{cases} 1.3 - 0.42\varepsilon & \text{N A30} \\ 1 & \text{N B50} \end{cases} \quad (10)$$

4. SCANNING ELECTRON MICROSCOPY STUDY OF FOAM

The reliability of Eq. (3) can be supported to some extent through the analysis of Scanning Electron Microscope (SEM) images of the foam structure before and after testing to investigate any potential damage. Since SEM operates at low pressure and high energy levels, initial tests were conducted at prolonged exposure to determine any detrimental effects; none were observed. Nonetheless, the SEM images shown represent a small part of the total bulk foam structure and the extent of any damage observed may not be representative of the whole sample. Samples were cut using a surgical knife.

As reported by Mills and Gilchrist[22] and discussed in Section 3.1, recovery would be slowed by loss of gas pressure within the foam cells and plastic damage in the cell walls. While diffusion of the gas through the cell window membranes is one mechanism, it may also be expected that, depending on strain levels and polymer matrix, evidence of ruptured cell walls could also be observed in the SEM images.

Table 8. Variance in elastic Young's modulus at different strain rate at 23 °C

N B50		N A30	
Strain Rate (hr^{-1})	**Elastic Modulus E* (MPa)**	**Strain Rate (hr^{-1})**	**Elastic Modulus E* (MPa)**
0.3044	6.52	0.308	0.97
3.020	7.79	3.050	1.29
54.64	10.08	30.5	2.04
540.7	10.81	305.0	2.78

Figure 7. Foam Young's modulus at various strain rates at 23 °C

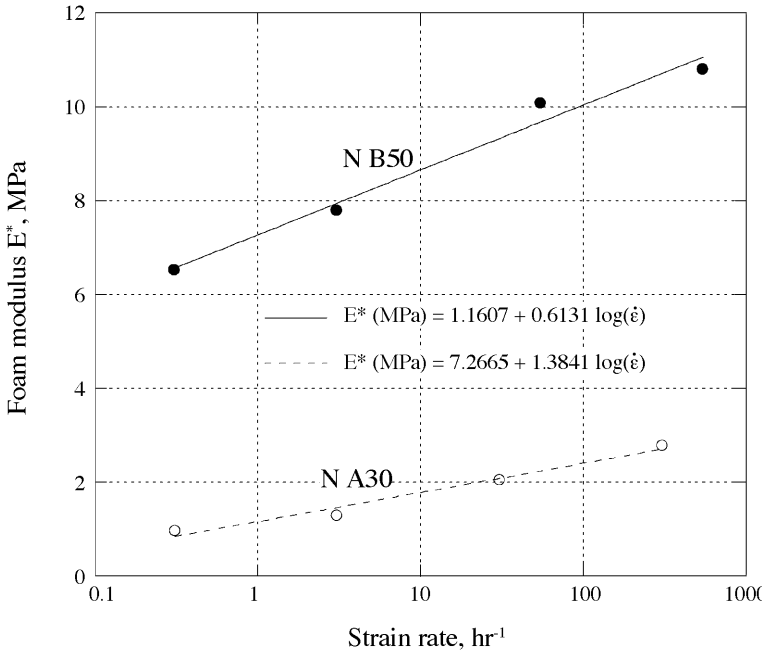

4.1 SEM Images Experimental Procedure

Compression set samples for 50% initial compressive strains were selected from the extremes of the temperature range. For comparative purposes, an uncompressed sample (zero compression) was also analysed as a control.

Three 10 mm X 10 mm X 5 mm (5 mm in direction of observation) test pieces were cut, from each of the compression set samples. The magnification settings are approximately 200x and 100x for the N B50 and N A30 images, respectively.

4.2 Interpretation and Discussion of SEM Images

SEM images of N A30 and N B50 at 50% strain are presented in **Figure 9a,c,d** and **f** for each of the compression set samples at both high (90 °C) and low (-5 °C) temperature. **Figures 9b** and **9e** show control samples which have experienced no compression testing. **Figure 9a-f** reveals no obvious damage in the form of burst cells. These images represent the extremes of test temperature and compressive strain for the compression set tests. Assuming these to be representative of the foam structure, it is reasonable

Figure 8. Experimental and fitted stress over the strain range 0.05 to 0.8 at 23 °C for the strain rates studied (a, b and c) N A30, (d) N B50

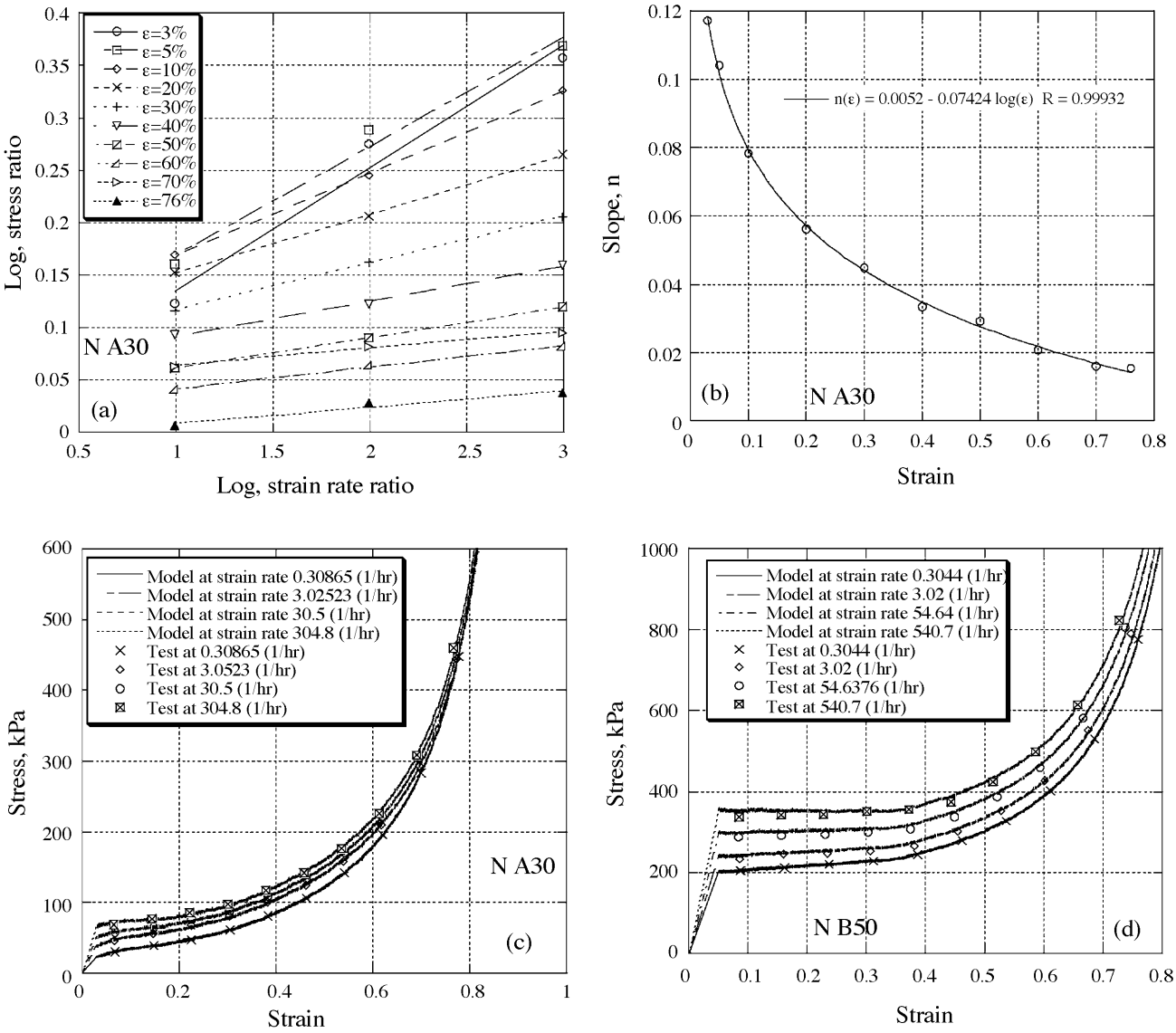

to assume no observable rupture of the cell windows would have been caused by the application of the lower strain levels and intermediate temperatures of the other compression set tests.

Figure 9a shows slightly more buckling and wrinkling within the polymer film than is observed in the control, **Figure 9b**. It is therefore possible that the N B50 foam will not recover its original thickness as some plastic damage may have occurred due to buckling in which the material has significantly exceeded the elastic limit of the polymer.

Figure 10a-d shows SEM images of the samples which have been compressed to 80% of the initial thickness during the compression tests for both foams. N B50 sample images show significant plastic damage resulting, in some cases, in rupture of the cell windows, **Figure 10a** and **10b**. This characteristic is also evident in the N A30 sample images with increased plastic damage but no observed bursting cell wall. These images confirm that the base polymer of N A30 foam has greater ductility than that of the more brittle N B50 polymer base, a result also indicated by the base polymer mechanical properties presented in **Figure 1b**.

5. DISCUSSION

The compression set data show that over a 24 hour period neither of the foam materials returned to its original thickness. This is expected behaviour of closed cell polymer foams, and suggests that mechanisms of plastic damage due to cell wall buckling and gas loss through diffusion have contributed to irrecoverable set in the bulk cellular structure. SEM images have identified that there is no

Figure 9. SEM results- 50% compression set tests (a) N B50 at 90 °C, (b) N B50 no compression at 23 °C, (c) N B50 at -5 °C, (d) N A30 at 90 °C, (e) N A30 no compression at 23 °C, (f) N A30 at -5 °C

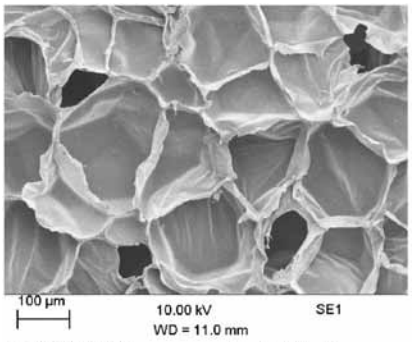

(a) N B50 50% compression @ 90 °C

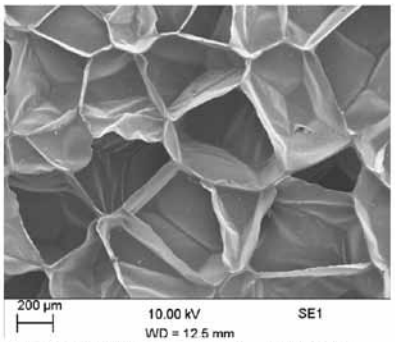

(d) N A30 50% compression @ 90 °C

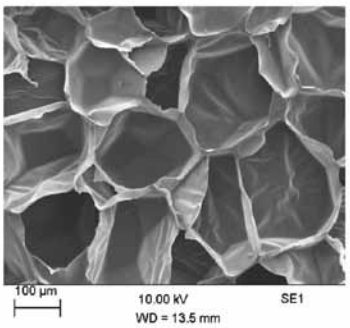

(b) N B50 no compression @ 23 °C

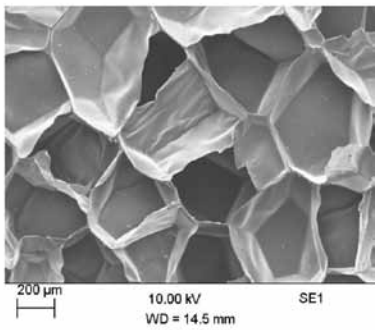

(e) N A30 no compression @ 23 °C

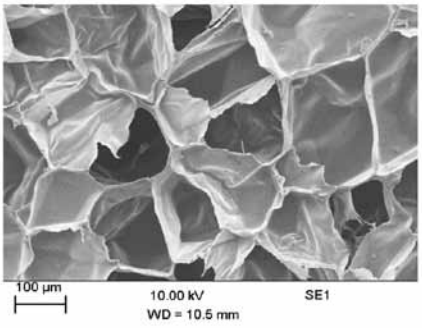

(c) N B50 50% compression @ -5 °C

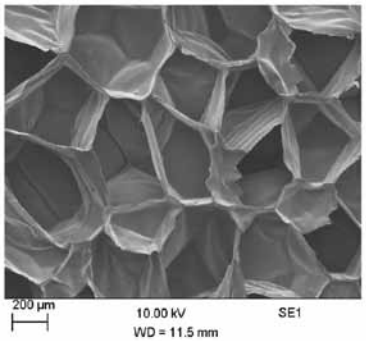

(f) N A30 50% compression @ -5 °C

consistent cell window rupture evident within the structure of the materials at strain up to 50%, but there are cell wall buckling effects visible in a number of the high strain samples. This is indicative of plastic damage caused by the initial compressive stage of the compression set test contributing to irrecoverable strain. Furthermore, the same behaviour was observed when additional N A30 samples were compressed to 80%. However, in N B50 samples under the same compression there was evidence of cell wall rupture which suggests that at strains greater than 50% compression cell walls did fail by this mechanism. This contributed to a reduction in the mechanical performance of the bulk foam. There is no evidence in this study to suggest that the foam material will not continue to recover beyond 24 hours since the base polymers are viscoelastic. It is reasonable to assume that, the foam would recover to, and then plateau, at some lower level of compression set, but that time frame far exceeds the limits of this study.

Figure 10. SEM results- 80% compression set tests (a) N B50 at 90 °C, (b) N B50 at -5 °C, (c) N A30 at 90 °C, (d) N A30 at -5 °C

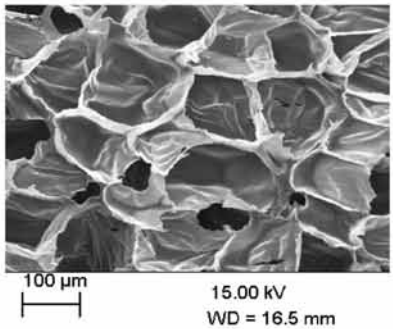

(a) N B50 80% compression @ 90 °C

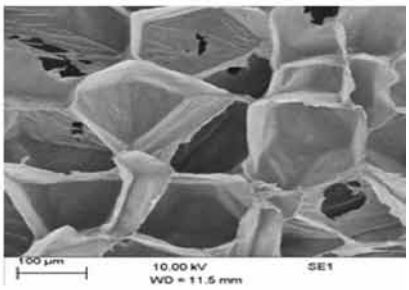

(b) N B50 80% compression @ -5 °C

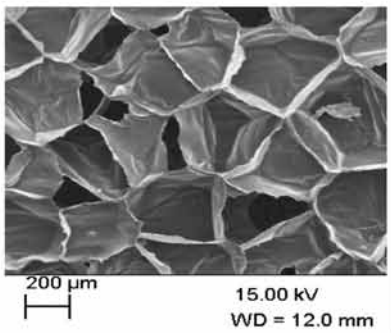

(c) N A30 80% compression @ 90 °C

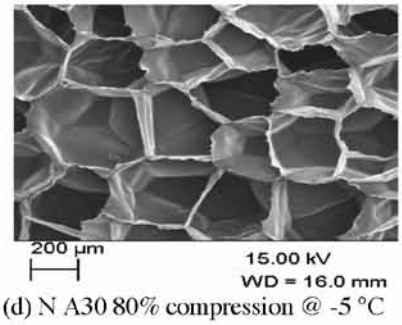

(d) N A30 80% compression @ -5 °C

Theoretically on application of the empirical Eq. (3), and assuming no plastic damage occurs, it could be predicted that the time required for the material to achieve a near zero compression set is measured in years.

Literature reports that the Tg of Nylon is approximately 50 °C[11,12]. It is noteworthy that on or around the Tg region, the mechanical properties of a polymer exhibited discontinuity in performance particularly in elastic modulus. Compression set results show anomalies at or around a temperature of 50 °C; compressive stress-strain data on the same foam indicate a local maximum around this point.

At temperatures near Tg the modulus of elasticity is sensitive to strain rate. In order to investigate this further, it would be necessary to measure the change in the elastic modulus as a function of strain rate at a constant temperature. This experimentation was carried out at four different strain rates, as discussed in Section 3. Over the strain rate range studied, the elastic modulus increases by approximately 100% and 200% for the N B50 and N A30 foams, respectively.

Stress-strain data were fitted as a function of strain rate using Nagy constitutive equation[30] for both N A30 and N B50. The fit for N B50 was found to be good. However, the fit for N A30 was not so good. Nagy's constitutive equation has been modified by including a strain dependent coefficient and the fit was much improved.

The modulus of elasticity and stress at particular strain values are sensitive to temperatures close to the glass transition[30]. Since polyamides are thermoplastics, literature indicates that the modulus of elasticity of the base polymer, and foams made from this polymer, may vary by 3 orders of magnitude dependent upon either change in temperature and or strain rate[2]. This study found that the elastic modulus tripled for N A30 and doubled for N B50 over the strain rate range studied, as shown in **Table 8**.

The manufacturing process of these foams incorporates a process by which the polymer base material is crosslinked[9]. It is reported[8] that the level of crosslinking vastly reduces the change in elastic modulus that can occur over the Tg region. It is postulated that the crosslinking characteristic may have limited the change observed in elastic modulus to approximately 200% over the ranges studied. This is beneficial in creating a consistent performance of such materials when operating at or above the Tg region, where otherwise performance may be highly variable. The sensitivity to compressive performance based on the level of crosslinking may vary depending on the polymer type.

In addition to crosslinking, this investigation has found that cell structure, polymer volume and the effect of gas pressure on these characteristics were also governing factors when predicting stress-strain performance of low density foams. This investigation found that the performance of low density foams was sensitive to temperature. WLF temperature shifting factors do not take into account the effect of the gas pressure-temperature dependency within the cell. In low density foam, the cell gas pressure can account for approximately 75% of the material's performance. For this reason any describing equation must include an additional term, based on the ideal gas law, which accounts for the effect of temperature on the gas within the cell. This then allows for the prediction of the combined behaviour of the polymer and gas within the cells, thus giving an accurate determination of bulk material stress-strain properties without the need for additional experimentation.

As stated by Zhang *et al.*[28], the Nagy and WLF equations can be linked to derive a combined strain rate and temperature equation for each material. Although, this theory has not been investigated in this work, it may be applicable using the developed Eq. (6) and (8) for each material. It should be noted that this must be supported with additional experimentation.

6. CONCLUSIONS

In this paper, time and temperature dependent predictive functions have been developed to approximate the compression set and recovery performance of two types of closed cell crosslinked polyamide-6 based foams. These equations are limited to the ranges studied, and any extrapolation beyond these limits would need to be supported by further experimentation.

The Nagy constitutive equation and WLF scaling factor have been applied to derive accurate strain rate and temperature dependent functions for both foams. The coefficients for the scaling equations are dependent on the temperature and strain rates and they are determined in this study for two foams.

From SEM studies, it was observed that at all temperatures samples compressed up to 50% strain do not show cell walls rupture. This confirms that all results for the 50% or less compression set tests are unaffected by temperature and therefore supports the application of empirical equation (Eq. 3).

SEM images of the N A30 foam samples show no significant damage in the form of cell wall rupture; even after 80% compression strain is achieved. However, buckling of the cell walls is evident. SEM images of the N B50 foam samples show evidence of cell wall rupture (approximately 10%) when 80% compression strain is achieved. This is consistent with differences in the ductility of the base polymers.

Both experimental and direct measurement has determined that for

the base polymers, the Tg is 48 ± 3 °C. This value is in agreement within the ranges given in literature for Nylon 6.

ACKNOWLEDGEMENTS

The authors would like to acknowledge the financial support from EPSRC for project CASE/CNA/06/29 and from Zotefoams plc. Many thanks go to the technical staff at Zotefoams plc for the supply of the samples and to Richard Giddens and Colin Bradsell for their technical expertise. In addition our thanks also go to Bryan Ruby and Trevor Nell for the manufacture of the compression test fixtures.

REFERENCES

1. Mills N.J., *Polymer Foams Handbook, Engineering and Biomechanics Applications and Design Guide*, 1st Edition, Chapter 7, Butterworth-Heinemann, 2007.
2. Gibson L.J. and Ashby F., *Cellular Solids, Structures and Properties*, 2nd edition, Pergammon Press, Oxford, 1999.
3. Kraynik A.M. and Warren W.E., *Low Density Cellular Plastics, Physical Basis of Behaviour*, 1st Edition, Chapter 7 - *The Elastic Behaviour of Low-Density Cellular Plastics,* Chapman and Hall, 1994.
4. Mills N.J., Stampfli R., Marone F. and Bruhwiler P.A., Finite Element Micromechanics Model of Impact Compression of Closed-Cell Polymer Foams, *International Journal of Solids and Structures*, **46** (2009) 667-697.
5. Mills N.J. and Zhu H.X., The High Strain Compression of Closed-Cell Polymer Foams. *Journal of the Mechanics and Physics of Solids*, **47** (1999) 669-695.
6. Mills N.J. and Hwang A.M.H., The Multiple - Impact Performance of High - Density Polyethylene Foam, *Cellular Polymers,* **9** (1989) 259-276.
7. Rodriguez-Perez M.A., Diez-Gutierrez S., De Saja J.A., The recovery behaviour of crosslinked closed cell polyolefin foams, *Polymer Engineering and Science*, **38** (1998), 831-837.
8. Ashby M.F. and Jones D.R.H., *Engineering Materials 2 – An Introduction to Microsctructures, Processing & Design,* 2nd edition, Butterworth and Heinemann, 1998.
9. www.zotefoams.com, *Date of Access February 2011*
10. BS 2782-3 METHODS 320A TO 320F, 1976 Incorporating Amendment No.1 *Plastics Part 3, Mechanical Properties - Methods 320A to 320F, Tensile Strength, Elongation and Elastic Modulus*.
11. Greco R., Nicodemo L. and Nicolais L., The Glass Transition of Nylon 6, *Macromolecules*, **9**(4) (1976) 686-687.
12. Mills N.J., *Plastics Microstructure, Properties and Applications,* Edward Arnold, 1986.
13. Park K.W., Kim G.H. and Chowdhury S.R., Improvement of Compression set Property of Ethylene Acetate Copolymer/ Ethylene-1-Butene Copolymer/ Organoclay Nanocomposite Foams, *Polymer Engineering and Science*, (June 2008) 1183.
14. Sreeja T.D. and Kutty S.K.N., Studies on Acrylonitrile Butadiene Rubber/Reclaimed Rubber Blends, *Journal of Elastomers and Plastics*, **34** (2002) 45.
15. Jhlham I.S. and Maita I.J., Testing and Evaluation of rubber-base Composites Reinforced with Silica Sand, *Journal of Composite Materials*, **40** (2006) 2099.
16. Nayak N.C. and Tripathy D.K., Studies on Composites Based on Acrylonitrile Butadiene Rubber and High styrene Resin, *Journal of Elastomers and Plastics*, **33** (2001) 179.
17. Bacci D., Marchini R. and Scrivani M.T., Peroxide Crosslinking of Ziegler Natta Thermoplastic Polyolefins, *Polymer Engineering and Science*, **44** (2004) 131.
18. Coons J.E., McKay M.D. and Hamada M.S., A Bayesian Analysis of the Compression Set and Stress-Strain Behaviour in a Thermally Aged Silicone Foam, *Polymer Degradation and Stability*, (2006) 1824.
19. Neff R.A. and Marsalko T.M., Roles of Convention Polyol and Isocyanate in Humid Aging and Durability of Molded seating Foam, *Journal of Cellular Plastics* **35** (1999) 492.
20. BS EN ISO 1856, 2001 Incorporating Amendments No 1, *Flexible Cellular Polymeric Materials – Determination of Compression Set.*
21. ASTM D395-03,2008 *Standard Test Methods for Rubber Property Compression Set*
22. N.J. Mills and A. Gilchrist, Creep and Recovery of Polyolefin Foams – Deformation Mechanisms, *Journal of Cellular Plastics*, **33** (1997) 264-292.
23. BS EN ISO 1923,1995 *Cellular Plastics and Rubbers – Determination of Linear Dimensions*
24. BS EN ISO 845,1995 *Incorporating Amendments No.1 Cellular Plastics and Rubbers- Determination of Apparent (Bulk) Density.*
25. Izzard V.G., Bradsell C.H., Hadavinia H., Morris V.J., Foot P.J.S. and Witten N., Investigation of the Compression Recovery Properties of Polyamide-6 Cellular Solid Over the Temperature Range of -5°C to 90°C, *Key Engineering Materials* **417-418** (2010) 933-936.
26. SYSTAT User Manual, *TableCurve 3D, Automated Surface Fitting and Equation Discovery Version 4.0 for Windows, 2002*.
27. BS EN 3386-1, 1998 *Polymeric Materials, Cellular Flexible Determination of stress-strain Characteristics in Compression, Low Density Material*.
28. Zhang J., Kikuchi N., Li V., Yees A. and Nusholtz G., Constitutive Modeling of Polymeric Foam Material Subjected to Dynamic Crash Loading, *Int. J. Impact Engineering* **21**, (1998) 369-386.
29. Nagy A., Ko W.L. and Lindholm U.S., Mechanical Behaviour of Foamed Materials under Dynamic Compression. *J. Cellular Plastics*, **10**, (1964) 127-134
30. Mano J.F. and Viana J.C., Effects at the Strain Rate and Temperature in Stress Strain Tests, Study of the Glass Transition of a Polymide – 6, Polymer Testing, **20** (2001) 937-943.